Korean J. Chem. Eng., **31**(2), 201-210 (2014)
DOI: 10.1007/s11814-013-0206-5

pISSN: 0256-1115
eISSN: 1975-7220

Evaluation of bubble suspension behavior in electrolyte melts

Minseong Kim*, Kangwook Kim*, Munkyeong Hwang*, Kyubo Kim, and Juhun Song*†**

*School of Mechanical Engineering, Pusan National University, Busan 609-735, Korea
**Pusan Clean Coal Center, Pusan National University, Busan 609-735, Korea
(*Received 29 April 2013 • accepted 11 October 2013*)

Abstract−The viscosity of a molten electrolyte mixture commonly used in direct coal fuel cells (DCFCs) was evaluated. The measurements were obtained from near the melting temperature to a high temperature at which a considerably bubbly flow was induced by decomposition. A gravity-driven capillary viscometer was employed to obtain the viscosity data under low Reynolds flow conditions, using a modified Poiseuille flow relationship. The importance of carbon dioxide addition in measuring the intrinsic viscosity was clearly observed. In addition, the effect of the bubble suspension on the viscosity was quantified in terms of the volume fraction and capillary number. The results showed that the increase in viscosity was best explained only by the difference in the volume fraction of spherical bubbles in the electrolyte melt.

Keywords: Direct Coal Fuel Cell (DCFC), Electrolyte Melt, Viscosity, Bubble Suspension, Volume Fraction

INTRODUCTION

There is growing interest in direct carbon fuel cells (DCFCs) which generate electric power directly from the electrochemical reaction of solid carbonaceous material with oxygen. DCFCs can use the existing molten electrolyte mixture commonly used in molten carbonate fuel cell (MCFC) systems. Their electrochemical performance strongly depends on several factors, such as the wettability of the anode with the electrolyte, the ion conductance of the molten electrolyte, and their contact behavior with coal particles [1]. Among these, the improvement of ion conductance would require a full understanding of the convective and molecular transport properties of electrolyte mixtures, such as viscosity and evaporation. Considering the porous nature of metallic foam anodes, coal suspended in molten electrolyte mixtures may flow into the anode under a laminar flow condition.

Under certain conditions in which decomposition and subsequent evaporation/boiling processes compete, volatile substances such as carbon dioxide (CO_2) evolve from the electrolyte. Such substances can be present as either bubbles in the dilute phase or as foam structures in the dense gas phase, especially when the dissociation pressure of CO_2 reaches a saturated value. As the volume fraction of the volatile matter increases under slow flow conditions, bubbles may not exist as individual particles, but may coalesce and become distributed in the foam structure. The higher surface tension caused by such liquid films might govern the macroscopic viscosity. Compared to simple bubbly flow, the latter state is termed slug flow, which is characteristically unsteady and unstable [2]. For this reason, the effect on viscosity has been not adequately modeled, and has been evaluated in only a few experiments [3-5]. As velocity increases, slug flow is typically transformed to annular flow and, eventually, to mist flow.

Under low flow conditions, the presence of individual bubbles in electrolyte melts could inadvertently increase the viscosity inside the DCFC system, which would result in convective transport loss to the anode and subsequent reduction in ion conductivity. In addition, the suspension of another solid material in the melt, i.e., coal, could sufficiently worsen the viscosity and stop the flow. To avoid this situation, a lower loading of coal in the hot slurry mixture may be required. Typically, research to improve ion conductivity near the anode has concentrated on a stagnant condition of MCFC systems. In the DCFC system, it may be more important to guarantee convective transport of the coal/electrolyte slurry prior to reaching the anode, particularly under the abovementioned reacting flow conditions, i.e., low Reynolds number flow with bubble formation [6,7].

Therefore, it is necessary to obtain viscosity data for the pure electrolyte and evaluate bubble effects on the viscosity over normal operating temperatures, which range from the melting temperature (400 °C) to 600 °C. Under low velocity flow conditions, strong shear does not work more effectively across the bubble than surface tension. In other words, this lower shear force compared to the stronger surface tension would not deform the bubble [8,9]. As a result, the bubble merely plays the role of a spherical solid in the suspending electrolyte, and its presence produces a thickened boundary layer that increases viscosity as the bubble volume fraction increases. Manga et al. proposed a relationship between viscosity and the gas bubble volume fraction, in which the viscosity increased by up to 50% in the presence of bubbles in a steady pipe flow [10]. The numerical prediction was validated against the experimental results of Rust and Manga in a rotating viscometer [11,12], and was compared against the prediction of Llewellin et al. [13]. However, the effects of bubbles on rheological behavior have primarily been observed in simple fluids such as water or oil with melting temperatures below atmospheric temperature.

Viscosity data are available in the literature for electrolyte melts with higher melting temperatures. However, the information is lim-

†To whom correspondence should be addressed.
E-mail: jxs704@pusan.ac.kr

ited to specific electrolyte mixtures and ranges of temperatures. Furthermore, most of the data for the electrolyte mixtures were obtained from an oscillating viscometer operated at high temperature. A rotating viscometer has also been employed with electrolyte melts, in which the principle of Couette flow was applied. In general, both apparatus are likely to produce high Reynolds number flows owing to the inherent rule incorporating high shear conditions. Of course, such higher velocities may induce better mixing and dispersion of the coal in the suspended liquid. However, the viscosity of any bubbly mixture may be underestimated because of the shear thinning effect that results from bubble deformation after a bubble is formed. In addition, those apparatus were found to be inadequate for coal slurries with coal particle diameters greater than 150 μm because of particle disintegration.

In contrast, a gravity-driven capillary viscometer may be more adequate for the viscosity measurements of electrolyte melts with bubble motion under these low Reynolds number conditions. Owing to the relatively low velocity, bubble deformation would be prevented. As described earlier, surface friction predominates over the elastic restoring force exerted on the bubble surface, which could provide conditions similar to those observed at the anodic surface of an actual DCFC system. Under these laminar conditions, it is necessary to investigate how the viscosity correlates with the volume fraction or other bubble parameters. The accurate measurement of bubble volume fraction is, therefore, a prerequisite for such analysis.

In this experiment, rheological behavior, such as viscosity, was evaluated for an electrolyte mixture under laminar flow conditions and over temperature ranges in which individual bubbles were induced. In particular, a gravity-driven capillary viscometer was employed to measure the steady-state velocity over the flow period. The combination of the velocity data with the Poiseuille flow relationship was further analyzed to obtain reliable viscosity values. The effect of CO_2 addition on the effective viscosity was observed. Finally, the dependence of viscosity on the volume fraction and capillary number was assessed for the bubbly electrolyte.

EXPERIMENTAL

1. Principles of Capillary Viscometry

Theoretical relationships allow for the determination of viscosity from velocity or velocity gradient data. For example, a relationship is well described in a handbook for commercial capillary viscometry [14]. In a capillary viscometer at a relatively low pressure difference between the inlet and outlet, an image is recorded to determine the time required for a defined liquid volume to be depleted after a flow. While the driving force is the hydrostatic pressure of the liquid column, it is possible to use over-pressure to achieve a higher velocity or shear rate. In another approach, gravity-driven capillary viscometry was used to evaluate the flow behavior of a coal/water slurry (CWS) with a higher content of coal. Coal particles greater than 150 μm were too large to be tested in a conventional rotational viscometer, in which particle disintegration due to high shear was observed [15].

Fig. 1(a) presents a schematic diagram of the gravity-driven capillary viscometer, placed inside an electric furnace, used in this study. The positions of CO_2 supply and melt sampling, and high speed camera are clearly seen in the figure. In Fig. 1(b), the part of electrolyte melt reservoir with capillary was magnified to indicate the flow regimes with possible bubble presence. It consisted of two parts: a 70 mL cylindrical funnel used as a reservoir and a capillary tube which generated lots of wall friction. The capillary tube was connected to the bottom of the reservoir with a blocking plug mounted at the bottom outlet. The capillary length was 100 mm with a 7 mm diameter. The funnel and capillary tube were filled with the electrolyte mixture while heating to the desired temperature, with the capillary outlet blocked. Then, the outlet was opened and the sample was allowed to drain. During the flow period, consecutive images were recorded at a frame rate of 1/100 s using a high speed camera. The volume changes of the electrolyte melt in the funnel over specific

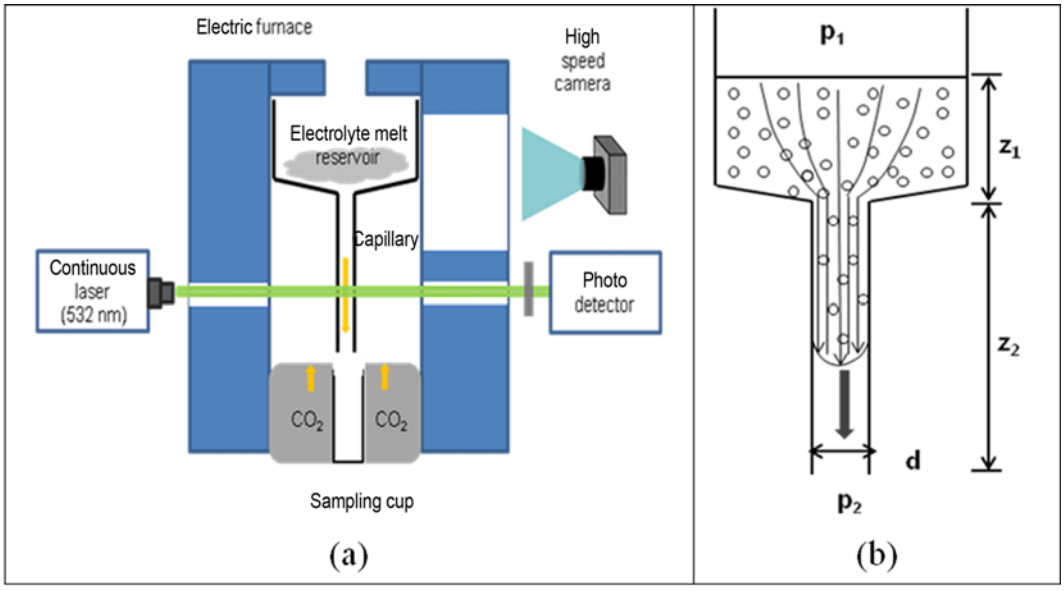

Fig. 1. Schematic of the experimental setup: (a) the capillary viscometer placed inside electric furnace equipped with measurement system such as laser and camera, (b) the electrolyte melt reservoir with capillary.

time intervals were measured to calculate the velocity, which was used to determine the final viscosity.

The first principle in capillary viscometry is given by the energy balance equation for incompressible viscous flow (Eq. (1)):

$$\frac{p_1}{\rho g}+\frac{V_1^2}{2g}+z_1+z_2=\frac{p_2}{\rho g}+\frac{V_2^2}{2g}+h_f \quad (1)$$

In this configuration, as both the inlet and outlet of the viscometer were exposed to the atmosphere, the pressure terms cancelled. The top surface at the inlet was assumed to be stagnant. A force balance equation is considered only for a differential control volume in a capillary tube with constant diameter. In Eq. (2), the viscosity is expressed in terms of frictional head loss rather than pressure loss. This is a slightly different form of the Poiseuille equation for laminar pipe flow [16].

$$\mu=\frac{\rho g d^2 h_f}{32 V_2 z_2} \quad (2)$$

After the rate of volume change was monitored over a steady-state period, the velocity was determined. With this value, the frictional head loss was calculated from Eq. (1), and the viscosity was calculated directly from Eq. (2). Then, the Reynolds number was calculated to determine whether the number was lower than 1000. If the Reynolds number was greater than 1000, the flow could be characterized as laminar, turbulent, or transitional, and the use of the above equations would be questionable [16].

Instead of the first method, which required frictional head loss, a wall shear stress was alternatively calculated according to the same procedure given in references [15] and [16]:

$$\tau_w=\frac{\rho g d}{4h_2}h_f=\frac{\rho g d}{4z_2}\left(z_1+z_3-\frac{v_2^2}{2g}\right) \quad (3)$$

The relationship of the shear stress to the frictional head loss was derived from the force balance equation for the integral volume inside a capillary tube. The frictional head loss was further related to the elevation head and head velocity after applying the energy balance equation for the entire viscometer. As an independent parameter, a strain rate was calculated at the wall from the measured average velocity using the following formula:

$$G_w=\left|\frac{dV}{dr}\right|_{r=R}=2\frac{V_{max}}{R}=\frac{8V}{d}=\frac{32\dot{Q}}{\pi d^3} \quad (4)$$

The ratio of wall shear stress to strain rate was alternatively used for viscosity analysis. This method provided identical viscosity results as the first method. In a pressure-driven capillary rheometer, there are some methods to correct raw viscosity data to the true viscosity by considering three effects: entrance and exit effect due to flow obstruction, namely, Bagley correction, slip effect at the wall (Mooney correction) and non-parabolic velocity distribution (Rabinowitsch correction) [17]. The Bagley correction is typically made to remove entrance effect by using pressure drop data from different length capillaries. In this study, the selection of the steady-state velocity eliminated any entrance and exit effect, which could accordingly provide a similar effect to the Bagley correction.

2. Measurement of Volume Fraction

A number of techniques are available to measure the average volume fraction of bubbles in a liquid with a low melting point temperature. They include optical scattering measurements, volume upheaval observations, and impedance measurements [18,19]. One of the simplest methods employs volume differences; a quick valve sampling method was used to stop and trap a bubbly phase in a given volume. Then, the trapped fluid was drained to measure the volume of fluid in the pure liquid phase. The ratio of the two volumes was interpreted as the volume fraction for the bubbly liquid. However, these techniques have not yet been confirmed for a bubbly electrolyte melt at relatively high temperatures.

We included a volumetric method to measure the volume fraction of bubbles in a stationary electrolyte mixture at relatively high temperature. The volume fraction was measured from the visual volume change by observing the uprising level of the top surface once decomposition initiated bubbling. As described earlier, the extent of bubbling depends on the saturation pressure of CO_2 gas in the atmosphere: Therefore, after the external CO_2 supply, *i.e.*, the bubble suppressant, was discontinued, the volume increased to a maximum level because of the gas bubble volume present in the liquid mixture. In this case, the volume fraction was defined by the ratio of the volume change at maximum to the mixture volume at the initial stage prior to bubble formation. Fig. 2 shows the temporal variation of electrolyte volume under a thermal cycle during which the atmospheric gases were changed from CO_2 to N_2, and back to CO_2 at a fixed temperature of 600 °C. After the initial heating and stabilization period at desired temperature under CO_2, the atmosphere was changed to N_2 to induce bubble formation, and changes in the volume were monitored. The CO_2 atmosphere was used for over 10 minutes, while N_2 was used for over 45 minutes.

The results of volume change showed the volume increased to a maximum value and then slowly decreased. The bell-shaped volume behavior may be attributed to two competing phenomena. The first is related to the decomposition reaction, which typically follows first-order kinetics. Initially, the rate of reaction accelerates, but slows down as the mixture becomes depleted. The second reason for the volume decrease after reaching the peak value arises from the bub-

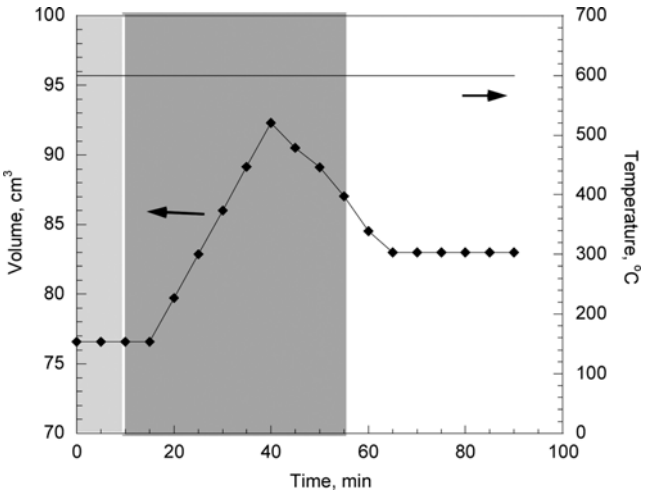

Fig. 2. Temporal variation of volume in the capillary viscometer at 600 °C. The light gray area indicates initial CO_2 atmosphere over 10 minutes; the dark gray area represents replacement by N_2 atmosphere for 45 minutes; and the white area indicates the restoration of CO_2 atmosphere.

ble loss mechanism involving bubble growth and attachment to the wall. As the number of bubbles and, therefore, the volume of the electrolyte melt increases, the bubbles are likely to move toward the wall and form a liquid layer known as a slug. Once this condition prevails, the further observation of any volume change fails owing to the severe opacity of the wall. Once the CO_2 atmosphere is restored, the volume returns to a constant value in absence of bubbles, as seen in the figure.

RESULTS AND DISCUSSION

1. Viscosity under CO_2-free Conditions

Under inert nitrogen atmosphere, i.e., CO_2-free conditions, the viscosity was measured for one electrolyte mixture at eight different temperatures in the capillary viscometer. The electrolyte mixture consisted of lithium carbonate (Li_2CO_3), potassium carbonate (K_2CO_3), and sodium carbonate (Na_2CO_3), blended in a 43.5 : 25 : 31.5 molar ratio. Compared to traditional binary mixture, lithium-potassium carbonate, this mixture is known to have much lower melting point and lesser segregation behavior because of sodium content [20]. The total mass of the mixture was 130 g, which maintained the reservoir height and, therefore, a constant elevation head. Because temperature is the primary parameter controlling ion conductivity under actual operating conditions, the temperature effect was first examined over the range 430-600 °C. The results in Fig. 3 show the raw data for reservoir volume change over time immediately after removal of the bottom plug. The rate of volume change represents the volumetric flow rate, which is related to the velocity. As the electrolyte mixture flows through a capillary with higher friction, it slowly accelerates and then flows at a constant steady state velocity. Toward the end of the capillary flow, an exit effect becomes prevalent, which accelerates the flow in a more vigorous way. In the plot, only the time interval with the fairly linear slope (at which the steady state velocity was achieved) was considered for the velocity derivation because of the presence of a fully developed region. For each temperature, the shaded box in the respective graph represents such a region in which the velocity became constant. After the rate of volume change was monitored over the steady state period, the velocity was determined. With the known velocity, the viscosity was then calculated using the modified Poiseuille Eq. (2).

In Fig. 4, the analyzed viscosity data are plotted against temperature and compared with experimental data measured in an oscillating viscometer from other work [21]. In their work, a viscosity relation with temperature was proposed after extrapolating viscosity data to lower limit, approximately 500 °C. Note that the lower limit was extended to near melting point, 430 °C in the present experiment. The viscosity measurements were repeated five times at each temperature, and averaged values and standard deviations were obtained. The experimental errors may be associated with processes such as the velocity determinations and density assumptions made

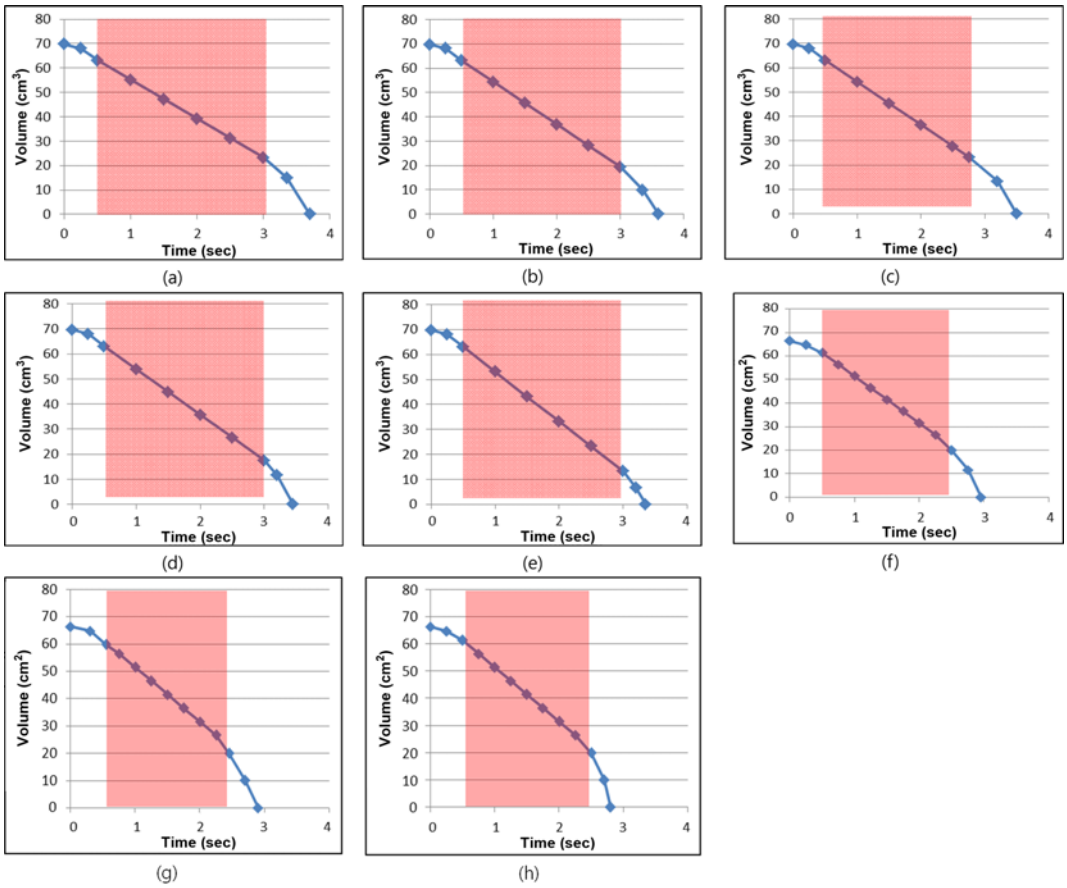

Fig. 3. Changes in reservoir volume measured under CO_2-free atmosphere at eight different temperatures: (a) 430, (b) 440, (c) 450, (d) 460, (e) 480, (f) 520, (g) 560, and (h) 600 °C.

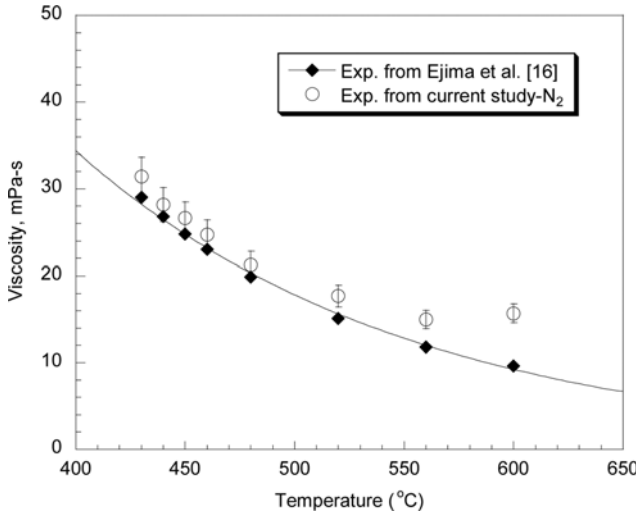

Fig. 4. Electrolyte melt viscosity measured under N_2 atmosphere (CO_2-free).

from an empirical relation. The error level at 95% confidence was within ±7% of the average viscosities for N_2 atmosphere and ±5% for CO_2 atmosphere as seen in the next section. The difference in magnitude of the average viscosities evaluated as a function of temperature was much greater than these error levels. This indicates that the data were statistically significant. The data for both viscometry methods were comparable in the low temperature range. However, when the temperature increased to a critical temperature of about 500 °C, the viscosity measured in the present experiment deviated from other data. This deviation can be attributed to the increase in the viscosity due to bubble suspension in the electrolyte melt. These bubble effects are further separated and quantified in the next section.

2. Effect of CO_2 Addition

In this experiment, the atmosphere was changed to 100% CO_2, while the other experimental conditions remained the same. The viscosity was measured in the capillary viscometer and similarly analyzed. The results in Fig. 5 present the raw data for the volume change over time at different temperatures. Steady state, fully developed regions with linear slopes describing volume changes were again observed. As described earlier, only the time interval with the fairly linear slope was considered for velocity derivation. The velocity data used for calculating the viscosity are listed in Table 1. Unlike the trend in slope change with increasing temperature under N_2 atmosphere, the slope continuously decreased with temperature under CO_2, leading to an exponential decay of viscosity with temperature. This indicated that bubbles did not contribute to the viscosity with increasing temperature. This behavior is clearly seen in Fig. 6, in which the viscosity was compared for both atmospheric conditions and reference data. Here, the temperature dependence of the vis-

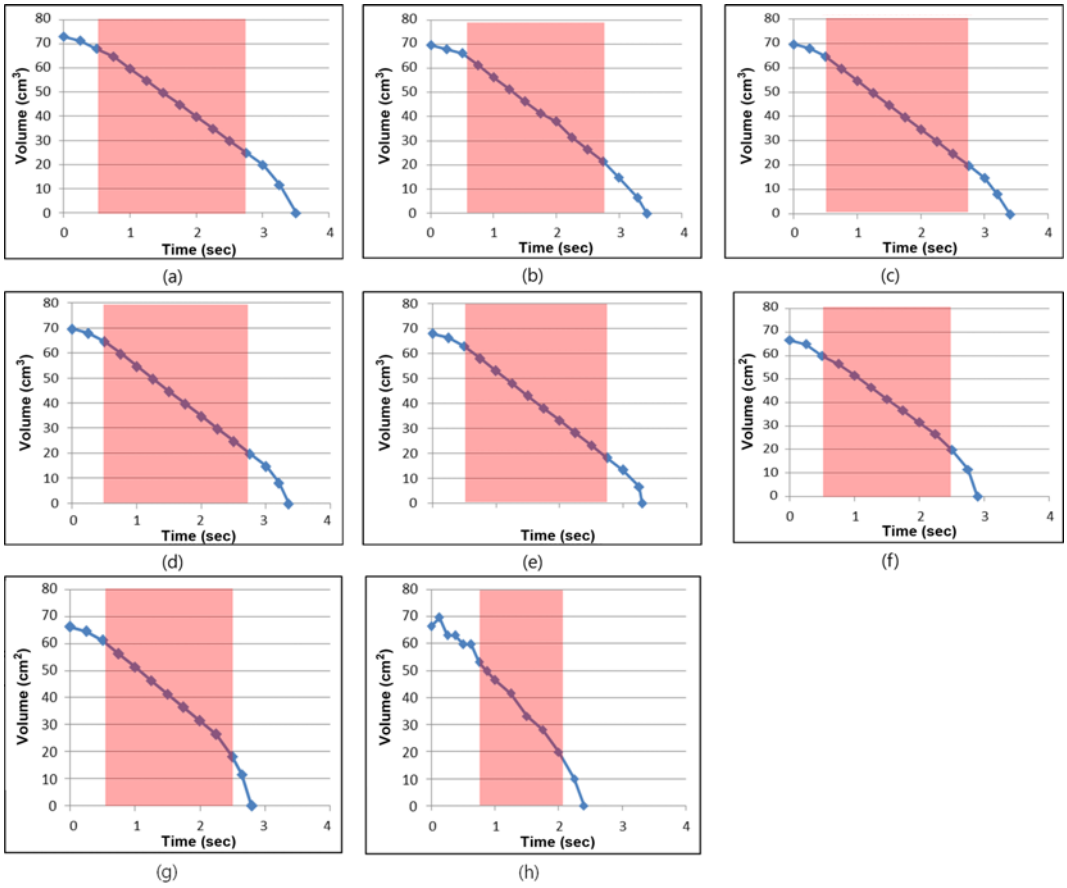

Fig. 5. Changes in reservoir volume measured under CO_2 atmosphere at eight different temperatures: (a) 430, (b) 440, (c) 450, (d) 460, (e) 480, (f) 520, (g) 560, and (h) 600 °C.

Table 1. Measured velocity data and resultant viscosity as function of temperature under CO_2 atmosphere

Temperature (°C)	Velocity (m/s)	Viscosity (mPa-s)
430	0.82	30.65
440	0.87	27.61
450	0.90	25.77
460	0.93	24.03
480	1.00	20.78
520	1.06	16.51
560	1.15	13.05
600	1.13	12.20

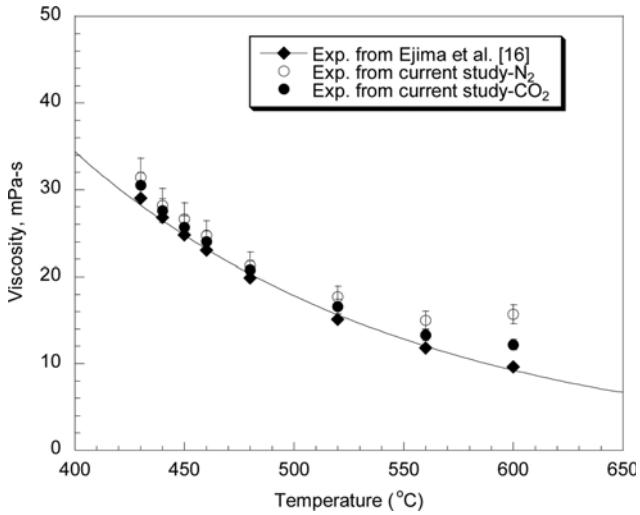

Fig. 6. Comparison of electrolyte mixture viscosities measured under different atmospheric conditions.

cosity under CO_2 atmosphere was fairly consistent with that reported in the reference [21].

We performed additional viscosity measurement at constant temperature (2nd highest temperature, 560 °C) where capillary diameters varied from 6 to 12 mm by the increment of 2 mm. While changing the shear stress with the capillary diameters, we evaluated the dependence of viscosity on the shear rate from the curves slope of shear stress versus shear rate. Fig. 7 illustrates how the viscosity varied against the shear rate under the two different atmospheres. The shear stress and shear rate were calculated using Eqs. (3) and (4), respectively. Whether or not a gas bubble formed, a fairly linear slope of the stress-shear rate curves was observed. The maximum error level was found to be ±10% for shear rate and ±3% for the shear stress. This indicated that the viscosity is independent of shear rate. This clearly confirmed that the electrolyte melts with bubble still conform to the Newtonian fluid behavior. In this regime, the velocity is parabolically distributed along the tube radius, which was not measured in this study [9]. The bubbly melt had a little greater viscosity than bubble-free melt. Interestingly, both curves were linearly extended to the origin within acceptable error levels. This indicated no yield stress behavior, which is another aspect of a non-Newtonian fluid.

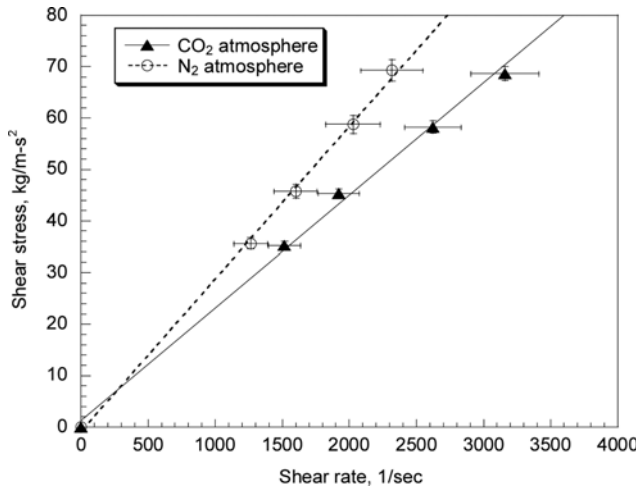

Fig. 7. Viscosity as a function of shear rate measured for electrolyte melt with/without a gas bubble at the same temperature condition, 560 °C.

The observed behavior of the Newtonian fluid over some ranges of shear rate and volume fraction may have a good reasoning from the theoretical consideration. As is known, there are some controversies on the mechanisms responsible for the reduced viscosity with the shear rate for the fluid with suspended particle. This behavior is a well-known characteristic of non-Newtonian fluids. One mechanism was related to bubble deformation by which the shear stress, otherwise fully transmitted to the fluid, was applied to deform or orient the single particle suspended in the medium. As the shear rate increased, elongated bubble reduced the viscous dissipation and thus viscosity due to higher presence of free slip surface ("slip effect"), as compared to reference condition with no bubble. In this mechanism, there was indeed critical shear rate (thereby the capillary number) where viscosity began to change with the shear rate [11]. We noticed that most of shear rate range considered in this study was well below the critical shear rate. The bubble was unlikely to be deformed in this shear rate condition. For this reason, we could infer that the bubbly electrolyte melt is in the Newtonian fluid regime.

The other mechanism to cause the reduced viscosity with shear rate was interactions between neighboring spherical particles so called "crowding effect" [22]. The effect was observed more prevalently in rigid sphere suspension. At low shear rate, viscosity was high because particle interactions, i.e., forces between colloidal particles induced coalescence. However, high shear overcame the inter-particle forces preventing the coalescence and thereby decreasing viscosity. This mechanism was pronounced with high concentration of particles suspended in the continuous medium. As this was, however, dilute state in this study (see the volume fraction data in Table 3), the reduction in viscosity hardly occurred under low shear rate. Therefore, the viscosity would not change significantly with shear rate and the bubbly electrolyte melt exhibited a Newtonian fluid behavior.

In brief, we strongly believe that the combination of low shear rate and concentration observed in this study could allow the bubbly electrolyte to follow the Newtonian fluid behavior. As is known, the non-Newtonian fluid would need additional correction on the viscosity by considering the effects such as Mooney and Rabinowitsch effect. The Mooney effect was encountered at slip condition either at a wall or near cylindrical bubble surface. The Rabinowitsch effect

produced a higher shear rate at the wall due to presence of non-Newtonian behavior. However, neither correction was required because of the prevalence of Newtonian fluid behavior [17].

3. Dependence of Viscosity on the Volume Fraction for a Bubbly Electrolyte

The effects of bubble shape, surface condition, and quantity on the viscosity were quantified for the previously discussed bubbly electrolyte melt. The capillary number, Ca, first needed to be defined for dilute suspensions in which bubbles were steadily formed. This dimensionless parameter defines the effectiveness of shear stress relative to surface tension at the bubble surface, and its magnitude determines how the bubble shape in the suspension affects the viscosity. At the zero shear rate limit (Ca→0), the bubble in the electrolyte melts remain spherical, while the bubble becomes deformed and elongated with a high shear rate and thus the capillary number. Another dimensionless parameter to affect the suspension viscosity is λ, which is defined as the ratio of the viscosity of dispersed phase to the viscosity of the continuous phase. This parameter may represent surface conditions of the bubble dispersed in the electrolyte melt. In this situation like gas bubble (inviscid or non-rigid particle) suspension, the λ is more likely to be zero. This differs significantly from the condition for a solid suspension where it is infinite.

From classical theory of suspension [11], a proportional constant term, f, in a simple relation of viscosity with volume fraction as expressed in Eq. (5) depends on Ca and λ. In other words, f is related to the properties of suspended particles such as the surface condition and structure of the bubbles.

$$\mu_{rel}=\frac{\mu}{\mu_{ref}}=1+\mathrm{f}(\mathrm{Ca},\lambda)\cdot\phi \tag{5}$$

Although there are some disputes over f values as the Ca approaches 0, f is reported to be dependent only on the surface condition (λ). In two extreme limits, f is constant at 2.5 with $\lambda=\infty$ for a rigid particle (solid and liquid) and at 1 with $\lambda=0$ for a non-rigid particle such as a gas bubble. This result is readily derived from the following Taylor's relation [23] in Eq. (6) generalized from Einstein's relation.

$$\mathrm{f}=\frac{\frac{5}{2}\lambda+1}{\lambda+1} \tag{6}$$

When Ca moves away from zero, the f value may still be positive, so that the presence of a suspension, such as bubbles, increases the relative viscosity in a linear function. As the Ca increases further, the f value tends to decrease. In particular, when Ca becomes infinite, f reaches a negative number. In the middle of the decrease, there is a critical Ca number at which f becomes negative. At this transition point, a shear stress starts to elongate the bubble, which then attenuates the viscosity because of the free slip surface around the slender bubble and reduced volume fraction of viscous fluid due to the presence of inviscid bubbles [11].

This means that the bubbles produce the opposite effect on relative viscosity when the deformation becomes predominant at high shear rate condition. Frankel and Acrivos developed a rheological model in which the critical Ca was 0.65 for Couette flow [24,25]. Murai et al. showed experimental results in which the critical Ca was retarded to a higher value (3.3). The deviation in the critical Ca was attributed to transient deformations of the bubbles during simple pipe flow [8].

Table 2. Prediction of capillary number (Ca) as function of temperature for bubbly electrolyte mixture

Temperature (°C)	Outlet velocity, V_2 (m/s)	Capillary number (Ca)
430	0.80	0.144
440	0.85	0.138
450	0.87	0.133
460	0.92	0.129
480	0.98	0.120
520	1.03	0.105
560	1.09	0.093
600	1.08	0.097

At each temperature tested for the bubbly electrolyte, the Ca was predicted using Eq. (7) given below. In a capillary tube, the strain rate at the wall is approximated as the average velocity divided by the tube radius, as shown in the section on viscometry principles. It was apparent that the parameters affecting Ca were the capillary diameter, the funnel height, and the bubble volume fraction. All of these would change the velocity, which would then affect shear stress. The computational results for the Ca are listed in Table 2.

$$\mathrm{Ca}=\frac{\tau}{\left(\frac{\sigma}{\mathrm{r}_b}\right)} \quad \text{where} \quad \tau=\mu\frac{\partial \mathrm{V}}{\partial \mathrm{y}}\approx\mu\frac{8\mathrm{V}}{\mathrm{d}} \tag{7}$$

The Ca values were within the range 0.097-0.144. When the computed values were compared with previously reported critical Ca values, they were always lower than either threshold value of 0.65 or 3.3. These were about five times lower than the former threshold [11]. In the low ranges of Ca, bubbles are not readily deformed and remain as spheres. The front blunt regions of the spherical bubbles will increase viscous dissipation and, therefore, the viscosity, unlike inner and slender regions of the bubbles. From this analysis, we may assume a constant value for f, and also that the bubbly fluid experiences negligible changes in shape. In this scenario, any increases in relative viscosity may occur solely by the displacement or amount of bubbles in the electrolyte melt. To verify such a hypothesis, the volume fraction of the bubbles was quantitatively measured using the simple volumetric method discussed in the experimental section. Table 3 lists the measured bubble volume fractions (ϕ), particularly at the four different temperatures at which bubbles were substantially observed. Like the viscosity measurements, the error levels for the bubble volume fractions were determined from repeated measurements, and were within ±8% of the average values.

The volume fraction of bubble was strongly associated with the rate of mass loss of the molten electrolyte mixture: the more the

Table 3. Volume fraction in bubbly electrolyte mixture measured by volumetric method

Temperature (°C)	Volume fraction
480	0.035
520	0.069
560	0.122
600	0.205

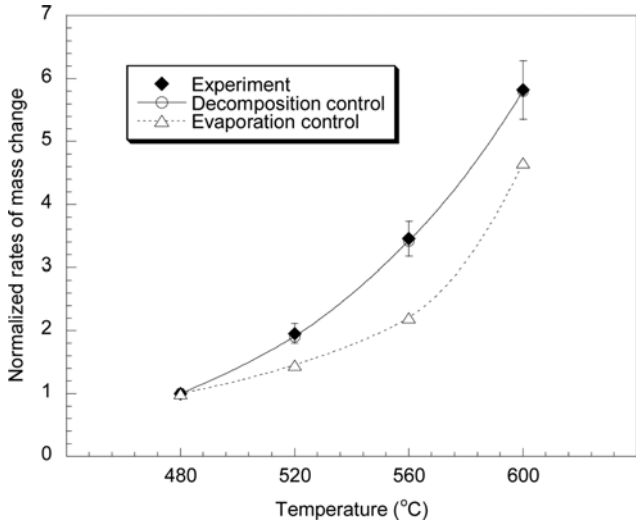

Fig. 8. Comparison of experimental volume fraction with rates of mass change theoretically predicted from two different modes: decomposition and evaporation process control.

electrolyte mixture lost in weight, the higher was the volume fraction. The steady weight loss from the electrolyte melt and the subsequent bubbly motion may involve several competitive processes, including decomposition reaction and evaporation or nucleate boiling processes [26,27]. While the electrolyte melt experiences thermal decomposition to the CO_2 vapor, bubble formation ensues in either slow evaporation or a fast boiling mode depending on saturation level of gas released in the melt. We speculated that an examination of the change in volume fraction with temperature could provide insight on the dominant rate process for the bubble generation. In Fig. 8, the experimental volume fraction is compared with mass loss rates computed from the decomposition control regime and evaporation control mode. The values were normalized to that at the lowest temperature (480 ºC). Three mechanisms and corresponding kinetic model to calculate the reaction rate of solid state decomposition have been well documented: Arrhenius's kinetic model, Knudsen-Langmuir's vaporization model, and Lvov's model [28]. Among them, the decomposition reaction rate was calculated using the simplest rate expression (8) available from the Arrhenius kinetic model [29,30]. The rate constant for the decomposition is in Arrhenius rate form and the order of reaction is first order.

$$\frac{dm}{dt} = -k(T)\cdot m \propto k(T) \quad \text{where} \quad k(T) = A\exp\left(-\frac{E_a}{R_u T}\right) \tag{8}$$

If the gas, CO_2, released from the electrolyte melt, is not fully saturated over the temperature ranges, the rate of electrolyte mass change may be limited by evaporation. This evaporation is caused by transport of the CO_2 gas in either bubble or by the gaseous diffusion from the vapor-liquid interface to the atmosphere. In this situation, gaseous diffusion is a rate-controlling process as the bubble transport of CO_2 gas would be relatively fast. Therefore, evaporation rate was calculated using planar natural evaporation model consistent with the gaseous diffusion, in which the vapor pressure at the interface was required [26,31]. The vapor pressure data at various temperatures were obtained in a separate experiment undertaken with a calcination furnace. The detailed description of the experimental method and relevant analysis can be found elsewhere [32].

$$\frac{dm}{dt} = -A_c\cdot\frac{\rho_v D}{L}\cdot\ln\left(\frac{1}{1-Y_v(T)}\right) \propto \ln\left[\frac{1}{1-Y_v(T)}\right]$$
$$\text{where} \quad Y_v(T) = \frac{p_v}{p}\cdot\frac{MW_v}{MW_t} \tag{9}$$

As another potential route, the gas released is saturated in the stationary electrolyte melt. This condition sustains bubble formation and subsequent fluid motion over the whole volume of the electrolyte, known as "nucleate pool boiling." While the mechanisms associated with this pool boiling phenomenon have been extensively studied, a complete model is yet to be developed [27]. This is mainly due to difficulties in predicting the number of bubble nucleation sites and the rate at which the bubble propels from each site. So, it was better here to use the most widely used correlations rather than to explore the bubble mechanism and resultant heat transfer rate in greater detail. One correlation was the theoretical relation developed by Rohsenow [33,34], where the heat rate scaled well with temperature to the 3 power. The precise expression was written in Eq. (10). In addition to some coefficients and exponent, most properties of vapor bubble and liquid appearing in the equation were independent of temperature.

$$\dot{q} = \mu_l h_{fg} A_c\left[\frac{g(\rho_l-\rho_v)}{\sigma}\right]^{1/2}\cdot\left[\frac{C_{pl}(T-T_{sat})}{C_{sf}h_{fg}Pr_l^n}\right]^3 \propto (T-T_{sat})^3 \tag{10}$$

In this case, the mass loss rate of electrolyte was accordingly calculated from the following form (11) and this rate yet had the temperature dependence of the 3 power:

$$\frac{dm}{dt} = \frac{\dot{Q}}{h_{fg}} \tag{11}$$

The comparison showed that the temperature dependence of the experimental volume fraction correlated best with that of the decomposition control mode. In this mode, the loss of electrolyte melt and the bubble suspension tends to increase exponentially with temperature. This is a conventional characteristic of a first-order decomposition reaction. Although the results are not shown in the figure,

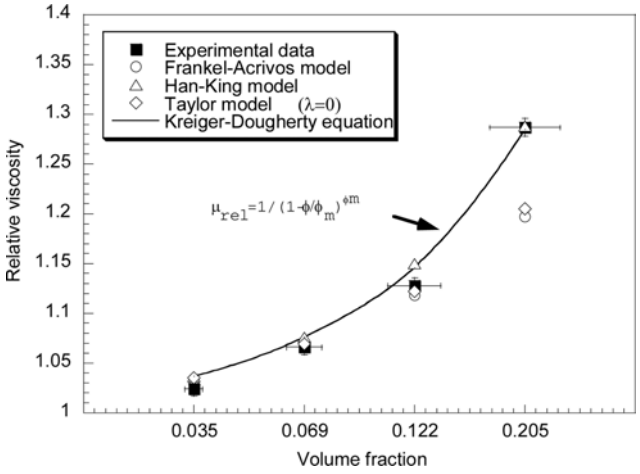

Fig. 9. Experimental relative viscosity as a function of volume fraction and comparison with theoretical predictions.

the values predicted from the nucleate boiling model were three orders of magnitude greater than the experimental values [27]. As a result, this analysis implied that the release of gaseous volatile matter and its bubble motion were controlled primarily by an early process of decomposition.

Fig. 9 presents the experimental relative viscosity data plotted against the measured volume fraction (ϕ). The relative viscosity is defined as the ratio of the viscosity of the bubbly electrolyte to the viscosity of the electrolyte under bubble-free conditions. The data are compared with theoretical predictions developed by Frankel and Acrivos [24] and Han and King [35] extended after the model of Choi and Schowalter [36]. Both theoretical Eqs. (12) and (13) relate the relative viscosity in terms of two parameters, such as Ca and volume fraction, and are valid for a colloid suspension such as gas bubbles, droplets, and solids in a dilute or semi-dilute concentration. In the equations, the Ca previously calculated was used, whereas the volume fraction was measured.

$$\mu_{rel}=\frac{1+\left(\frac{6}{5}\mathrm{Ca}\right)^2+\phi\left(1-\frac{12}{5}\mathrm{Ca}^2\right)}{1+\left(\frac{6}{5}\mathrm{Ca}\right)^2} \tag{12}$$

$$\mu_{rel}=\frac{1+\left(\frac{6}{5}\mathrm{Ca}\right)^2\left(1+\frac{20}{3}\phi\right)(1+4\phi)}{1+\left(\frac{6}{5}\mathrm{Ca}\right)^2\left(1+\frac{20}{3}\phi\right)^2}\left(1+\phi+\frac{5}{2}\phi^2\right) \tag{13}$$

The comparison of experimental relative viscosity with other models showed that Krieger-Dougherty model [22] or Han and King model provides the best regression fit for the experimental data of viscosity with the volume fraction. Note that the former is an empirical model from the experimental data and the latter is a model with theoretical validation. Because of the prevalence of Newtonian fluid at most ranges of shear rate, the shear rate would not affect the relative viscosity, which is evident in Eq. (14) of the Krieger-Dougherty model. Similar results were found in Rust's work [11] where the relative viscosity below the critical shear rate was predicted more accurately by this Krieger-Dougherty model. Therefore, the bubble deformation effect and resultant shear layer alteration could be completely excluded.

$$\mu_{rel}=\frac{1}{\left(1-\frac{\phi}{\phi_m}\right)^{\phi_m}} \tag{14}$$

In contrast, the prediction from the Taylor model [23] in the previous Eq. (6) with λ=0 deviated a little from the experimental data. Again, the model assumed an inviscid gas bubble for the suspended phase. The distinct deviation was observed with the Frankel-Acrivos model, particularly at high volume fraction.

The temperature dependence of molten electrolyte has been studied [21], but the dependence on the bubble fraction has not yet been studied. The data combined here provided valuable information on the viscosity relation with temperature as well as volume fraction. For example, we developed the viscosity model of bubble-free melt to predict its change with temperature over wide temperature ranges commonly used in the practical operation of the DCFC. This was made with exponential fitting for the measured data under the CO_2 atmosphere in Fig. 6. The effective viscosity model in Eq. (15) was then proposed for the present bubbly electrolyte mixture by combining the model with the relative viscosity equation.

$$\mu(\mathrm{T},\phi)=\mu_{ref}\times\mu_{rel}=0.2386\exp(28087/\mathrm{R}_u\mathrm{T})\times\frac{1}{\left(1-\frac{\phi}{\phi_m}\right)^{\phi_m}} \tag{15}$$

Overall, the analyses implied that the viscosity of the bubbly electrolyte melt was properly predicted only with an increase in the volume fraction. This was particularly pertinent for conditions in which the density of the bubble suspension was relatively low and bubble deformation was not involved owing to relatively low shear stress.

CONCLUSION

We evaluated the rheological behavior (such as viscosity) of electrolyte mixtures with and without bubble motion at relatively high temperatures (beyond their melting points). A gravity-driven capillary viscometer was used to obtain viscosities and bubble volume fractions under low Reynolds number flow conditions. The effects of CO_2 addition on viscosity were observed. For bubbly electrolyte melts under these flow conditions, the effect of bubble suspensions on the relative viscosity was quantified in terms of volume fraction and capillary number. A proposed correlation of the relative viscosity with the volume fraction provided much closer agreement with the experimental results.

ACKNOWLEDGEMENTS

This work was supported by a National Research Foundation of Korea (NRF) grant funded by the Korean government (MEST) (No. 2010-0019543). Some of the results are the outcome of another program (No. 2012R1A1A2002669), also supported by the NRF. Finally, the authors thank the Korean government (MKE) for financial support from the man power program (No. 20124010203230).

NOMENCLATURE

p : pressure [N/m^2]
g : gravity acceleration [m/s^2]
d : capillary tube diameter [m]
z : elevation [m]
V : average velocity [m/s]
h : head loss [m]
G : strain or shear rate [1/s]
R : capillary tube radius [m]
$\dot{Q}$: volumetric flow rate [m^3/s]
$\dot{q}$: heat transfer rate [J/s]
m : electrolyte mass [kg]
f : proportional constant
Ca : capillary number
r : radius [m]
k : reaction rate constant [1/s]
A : frequency factor [1/s]
E_a : activation energy [kJ/mol]
R_u : universal gas constant [kJ/mol-K]
A_c : capillary area [m^2]

h_{fg} : heat of vaporization [kJ/kg]
Y : mass fraction
MW : molecular weight [kg/kmol]
C_p : specific heat capacity at constant pressure [kJ/kg-K]
Pr : Prandtl number
C_{sf} : boiling constant between surface-fluid interface (=0.01)
T : temperature [K]
T_{sat} : saturation temperature [K]
D : mass diffusivity [m^2/s]
n : boiling exponent between surface-fluid interface (=1)
L : length [m]

Greek Characters

ρ : density [kg/m^3]
μ : electrolyte melt viscosity [cPs or mPas]
τ : shear stress [kg/m-s^2]
Δ : change of mass or volume for electrolyte melt
ϕ : volume fraction of bubbles in suspension
ϕ_m : maximum volume fraction of bubbles (=0.6)
σ : bubble surface tension [N/m]

Subscripts

1 : top of capillary viscometer
2 : bottom of capillary viscometer
f : wall friction
w : wall
max : maximum
l : liquid phase
g : gas phase
v : vapor phase
o : initial state before bubble formation
rel : relative to bubble-free condition
ref : bubble-free reference condition
b : bubble
m : maximum
t : total mixture
fg : phase change from liquid to gas
sat : saturation

REFERENCES

1. X. Li , Z. Zhu, J. Chen, R. Marco, A. Dicks, J. Bradley and G. Lu, *J. Power Sources*, **186**, 1 (2009).
2. Wolverine Tube Inc., *Void fractions in two phase flows*, in *Engineering Data Book III*, Available Online (2007).
3. N. D. Denkov, S. Tcholakova, K. Golemanov, V. Subramanian and A. Lips, *Colloids Surf.: A Physicochem. Eng. Aspects*, **282**, 327 (2006).
4. R. Hoehler and S. Cohen-Addad, *J. Phys. Condens. Matter*, **l17**, 1041 (2005).
5. Q. Xu and W. R. Rossen, *Colloids Surfaces: A Physicochem. Eng. Aspects*, **216**, 175 (2003).
6. G. A. Hackett, J. W. Zondlo and R. Svensson, *J. Power Sources*, **168**, 111 (2007).
7. D. Cao, Y. Sun and G. Wang, *J. Power Sources*, **167**, 250 (2007).
8. Y. Murai and H. Oiwa, *Fluid Dynamics Research*, **40**, 565 (2008).
9. M. Kameda, T. Katsumata and M. Ichihara, *Fluid Dynamics Research*, **40**, 576 (2008).
10. M. Manga and M. Lowwenberg, *J. Volcanol. Geothermal Res.*, **105**, 19 (2001).
11. A. C. Rust and M. Manga, *J. Non-Newtonian Fluid Mech.*, **104**, 53 (2002).
12. A. C. Rust and M. Manga, *J. Colloid Interface Sci.*, **249**, 476 (2002).
13. E. Q. Llewellin and M. Manga, *J. Volcanol. Geothermal Res.*, **143**, 205 (2005).
14. I. H. J. Wilke, I. H. Kryk, I. J. Hartman and W. Wagner, *Theory and praxis of capillary viscometer*, Chapter 2, Available Online (2007).
15. G. A. Nunez, M. I. Briceno, D. D. Joseph and T. Asa, *Colloidal coal in water suspensions*, Available Online (2005).
16. F. M. White, *Fluid mechanics*, 2nd Ed., McGraw-Hill (2001).
17. F. A. Morrison, *Shear viscosity measurement in a capillary rheometer*, Available Online as Lecture Note (2007).
18. J. Sowinski and M. Dziubinski, *Proceedings of European Congress of Chemical Engineering (ECCE-6)*, Copenhagen (2007).
19. G. F. Hewitt, in *Handbook of Multiphase Systems*, G. Hetsroni, Ed., McGraw-Hill, New York (1982).
20. Electrolyte, http://www.doitpoms.ac.uk/tlplib/fuel-cells/mcfc_electrolyte.php, Available Online (2013).
21. T. Ejima, Y. Sato, T. Yamamura, K. Tamal and M. Hasebe, *J. Chem. Eng. Data*, **32**, 180 (1987).
22. I. M. Kreiger and T. J. Dougherty, *Trans. Soc. Rheol.*, **3**, 137 (1959).
23. G. I. Taylor, *Proc. R. Soc. London, Ser. A*, **138**, 41 (1932).
24. N. A. Frankel and A. Acrivos, *J. Fluid Mech.*, **44**, 65 (1970).
25. E. J. Hinchi and A. Acrivos, *J. Fluid Mech.*, **98**, 305 (1980).
26. B. V. L'vov, *Thermochim. Acta*, **386**, 1 (2002).
27. F. P. Incropera and D. P. DeWitt, *Fundamentals of heat and mass transfer*, Chapter 10, 6th Ed., Wiley (2006).
28. B. V. L'vov, *J. Thermal Anal. Calorimetry*, **96**, 487 (2009).
29. S. R. Turns, *Introduction to combustion: Concepts and applications*, Chapter 3, 2nd Ed., McGraw-Hill (2000).
30. K. H. Stern and E. L. Weise, *National Bureau of Standards*, **30** (1969).
31. B. V. L'vov, *Thermochim. Acta*, **373**, 97 (2001).
32. S. C. Lee, M. S. Kim, M. K. Hwang, K. B. Kim, C. H. Jeon and J. H. Song, *Experiments in Fluid and Thermal Science*, **49**, 94 (2013).
33. W. M. Rohsenow, *Trans. ASME*, **74**, 969 (1952).
34. R. I. Vachon, *J. Heat Transfer*, **90**, 239 (1968).
35. C. D. Han and R. G. King, *J. Rheol.*, **24**, 213 (1980).
36. S. J. Choi and W. R. Schowalter, *Phys. Fluids*, **18**, 420 (1974).